Large-Scale Simulation of the Human Arterial Tree

L. Grinberg[1], T. Anor[2], J.R. Madsen[2],
A. Yakhot[3] and G. E. Karniadakis[1,*]

[1]Division of Applied Mathematics
Brown University, Providence, RI

[2]Children's Hospital
Harvard Medical School, Boston, MA

[3]The Pearlstone Center for Aeronautical Engineering Studies,
Department of Mechanical Engineering
Ben-Gurion University, BeerSheva, Israel

short title: Simulation of the Human Arterial Tree.

*corresponding author. Box F, Division of Appl. Math., Brown University, Providence, RI 02912. Tel. +1 (401) 863 1217; fax +1 (401) 863 3369; e-mail gk@cfm.brown.edu.

SUMMARY

1. Full-scale simulations of the virtual physiological human (VPH) will require significant advances in modeling, multiscale mathematics, scientific computing and further advances in medical imaging . Here, we review some of the main issues that need to be resolved in order to make three-dimensional (3D) simulations of blood flow in the human arterial tree feasible in the near future.

2. A straight-forward approach is computationally prohibitive even on the emerging petaflop supercomputers so a three-level hierarchical approach based on the vessel size is required consisting of: a Macrovascular Network (MaN), a Meso-vascular Network (MeN), and a Microvascular Network (MiN). We present recent simulations of MaN obtained by solving the 3D Navier-Stokes equations on arterial networks with tens of arteries and bifurcations and accounting for the neglected dynamics through proper boundary conditions.

3. A multiscale simulation coupling MaN-MeN-MiN and running on hundreds of thousands of processors on petaflop computers will require no more than a few CPU hours per cardiac cycle within the next five years. Rapidly growing capacity of supercomputing centers opens up the possibility of simulation studies of cardiovascular diseases, drug delivery, perfusion in the brain, and other pathologies.

Key words: CFD, bioflows, multiscale modeling, medical imaging.

INTRODUCTION

Computational Fluid Dynamics (CFD) enables accurate simulations of blood flow in arterial bifurcations, stented vessels, arteries with aneurysms or stenoses, among others. Results of these CFD simulations may help in understanding the biomechanics of such pathologies and accelerate their use in pre-surgical computer-assisted planning [1, 2, 3, 4, 5]. Similarly, CFD simulations of blood flow in entire vascular networks will lead to a better understanding of oxygen transport to the tissues and the brain, and in designing more effective procedures for drug delivery [6, 7]. In recent years, numerous works have been devoted to CFD modeling of arterial flows , but most of them are limited to one or two arteries only [8, 9, 10, 11, 12, 13, 14].

Interactions of blood flow in the human body occur between different scales, in which the large-scale flow features are being coupled to cellular and sub-cellular biology, or at similar scales in different regions of the vascular system [15, 16, 17, 18, 19]. At the *largest scale*, the human arterial system is coupled through the wave-like nature of the pulse information traveling from the heart into elastic arteries. Surgical interventions, such as bypass grafts, leading to a change in the arterial network alter the wave reflections, which, in turn, can modify the flow waveforms at seemingly remote locations. Subsequently, the modification of a local waveform can lead to the onset of undesirable wall stresses, which could start another pathological event. At the *cellular scale*, the blood cell that plays a central role in the blood clotting process is the platelet [20]. Blood vessels injured by smoking, cholesterol, or high blood pressure develop cholesterol-rich plagues that line the blood vessel wall; these plagues can rupture and cause the platelets to form a clot which leads to a blockage of blood flow. In arteries of the heart, the process leads to chest pain and heart attack; in arteries of the neck and brain, the process causes strokes. Simulations of this clotting process at the atomistic level have been recently presented in [21, 22].

Numerical simulations of such pathologies require *multiscale modeling* across many orders of magnitude of spatial and temporal scales. Indeed, there is the prospect of coupling multiscale representations of blood flow, ranging from a quasi 1D transient flow in compliant vessels at the largest scale, to unsteady 3D flows in curved and flexible vessels at the mm range, to multi micron-scale thrombus formation at a fissure in the lumen of such a vessel with an atherosclerotic plaque. The main challenge of simulating the blood flow interactions, from the scale of the entire human arterial tree down to the scale of platelet aggregation, lies in the high demand such a task places on supercomputing. High performance computing is essential to modeling the three-dimensional unsteady fluid mechanics within sites of interest such as arterial branches and the process of platelet aggregation and thrombosis with tens of millions of platelets.

A simple estimate of the enormous resolution required can be obtained as follows: assuming that we use a tetrahedral elements to descritize the typical blood volume for a human (5 liters), with a $0.5mm$ edge for each tetrahedron (and corresponding volume of $0.0147\,mm^3$) we will require more than 339 million finite elements. For
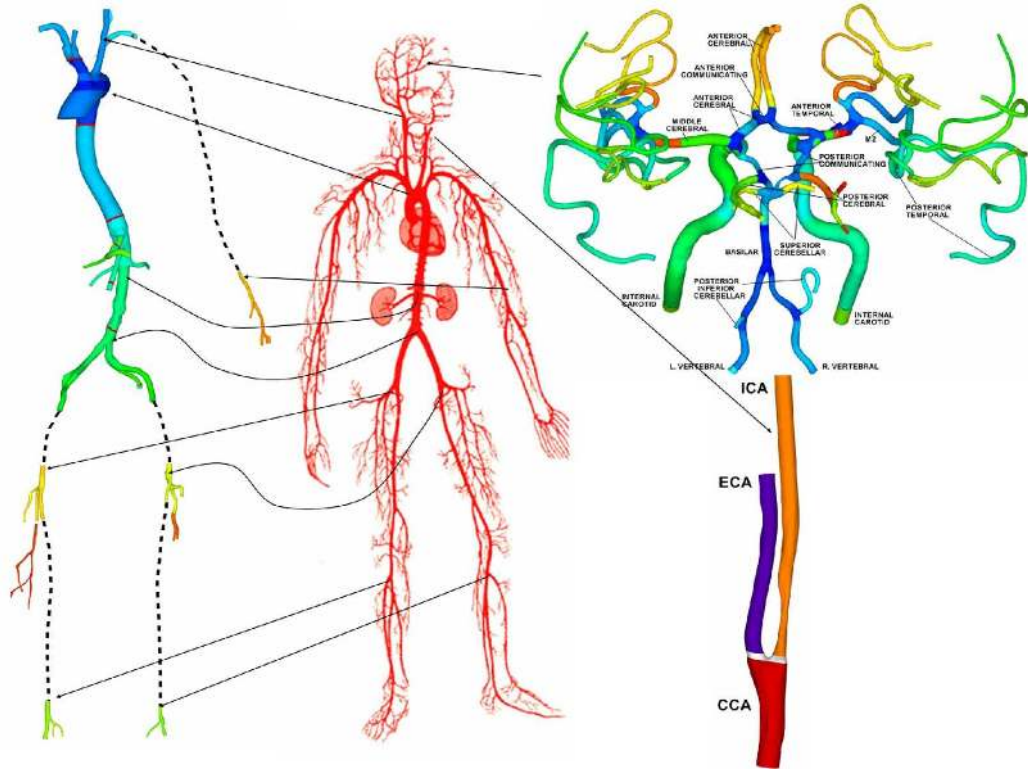
Figure 1: 3D model of major vessels and bifurcations of the human arterial tree reconstructed with gOREK from a set of CT, DSA CT and MRA images. Colors represent different parts of the model. Left: Aorta and adjacent arteries. Right top: Cranial arterial network. Right bottom: Carotid artery.

high-order discretizations, such as spectral/hp elements, the number of required grid points is then $339M \times (p+3)(p+2)^2$, which for (polynomial order) $p = 4$ results in about 85.5 billions of grid points – an enormous number indeed! Since 20% of this blood is in the brain, a tesselation of the cerebrovasculature requires 67.8 million elements or 17.1 billions of grid points. This estimate is admittedly conservative as it is based on a uniform discretization of arteries, arterioles and capillaries. A further simplification can be made if we treat the venular system, containing about 75% of the blood, as a large reservoir. However, such estimate points to the fact that at the present time, even with petaflop computing resources (performing up to 10^{15} operations per second), the brute force approach of a *full* 3D simulation at all scales is not feasible, and hence a new *hierarchical* modeling approach for the human arterial tree is required; such modeling reduces the problem size and corresponding computational complexity, and can be characterized by three distinct *spatial* length scales:

1. *The macrovascular network (**MaN**) consisting of large arteries*, down to diameter of 0.5 mm, which are patient-specific and can be reconstructed from clinical imaging.

2. *The mesovascular network (**MeN**) consisting of small arteries and arterioles,*

from 500 μm down to 10 μm, which follow a tree-like structure governed by specific fractal laws [23, 24]. For example, the human brain contains about 10 million small arteries and arterioles (this number is computed based on Murray's law [25, 26] with a modified index ($q = 2.5$) and asymmetric structure).

3. *The microvascular network (**MiN**) consisting of the capillary bed*, which follows a net-like structure. Its topological statistics have recently been quantified for the human brain in [23]. The typical number of capillary segments in the brain is more than 1 billion.

In order to make progress in simulating the human arterial tree this hierarchical approach should involve simulations of two regimes: The first one includes all arteries that can be accurately imaged clinically at the present time (e.g., MaN), see figure 1. The second regime includes the "subpixel" dynamics (MeN and MiN as described by (2) and (3) above) acting as "closure" to the large scale arterial dynamics (MaN). Today accurate simulations of the entire MaN are possible on the emerging petaflop computers while significant simplifications are required for simulating MiN and MeN.

During the last two decades, most studies of bioflows consider a single bifurcation as a model geometry. Recently, the widely available parallel computers, mostly in the form of PC clusters, and their increasing use in biomechanics has led to simulations with multiple bifurcations [27, 28, 29, 30] and even full-scale arterial trees on the super-cluster of distributed computers, such as the TeraGrid[31], involving more than 20 bifurcations computed on thousands of processors [32].   Such geometrically complex arterial networks involve many inlets and outlets and unless the closure problem is solved by simulating both MeN and MiN - a rather formidable task at present - proper boundary conditions should be employed to account for the neglected dynamics downstream. Another important issue is the accuracy of geometric data acquisition, due to the geometric complexity of most arteries as well as the flexibility of the arterial walls.

In this paper we review recent progress on simulating arterial trees with emphasis on large-scale simulations of blood flow in arterial networks. The paper is organized as follows. In the section Medical Data Acquisition we discuss existing data acquisition techniques and methods for validation and for data assimilation, i.e., incorporating clinical data in CFD simulations. In the section Numerical Models we review existing numerical methods and present representative results. In the last section we conclude with a brief outlook on what may happen in the next decade or so in the field of large-scale simulation of arterial networks.

MEDICAL DATA ACQUISITION

In this section we briefly review existing techniques for collecting and processing medical data that is used in CFD simulations. These data typically include: (a)

geometry of the vascular network, (b) flow and pressure boundary conditions, and (c) material properties of the vessels and the blood. We will only discuss (a) and (b) here.

Reconstructing vascular networks from medical images

Several techniques for obtaining information of arterial geometries exist:

Computed tomography (CT): This method is based on the idea of the Italian radiologist Alessandro Vallebona who first suggested in the 1930s that it is possible to map a slice of a human body on a radiographic film. CT produces two-dimensional (2D) images (slices) of a human body, which, upon assembly in a 3D field, demonstrate various structures (organs) based on their ability to block the X-ray beam. CT *angiography* is an enhancement of the method, where a contrast material is injected into the blood to allow clear capturing of the blood volume and thus detection of the shape of the vessels' internal wall.

Digital subtraction angiography CT, (DSA CT): This is a recent enhancement of the CT technique allowing a seamless 3D-based digital separation of vessels from the bones [33, 34]. This method is particularly valuable for visualization and reconstruction of the cranial arterial network.

Magnetic resonance angiography (MRA): MRA is based on magnetic resonance imaging and provides images with superior contrast resolution compared to CT. The drawback of the MRA method for arterial shape reconstruction is its inability to capture a volume where blood is stagnant, since the method is based on detecting a moving fluid.

The aforementioned methods provide a set of 2D images which upon integration into a 3D data set is processed using different numerical procedures. The reconstruction of arterial wall geometries is based on analysis of the data encoded in the images. Two common approaches for arterial wall identification are: (a) level set method - a numerical technique for identifying interfaces and shapes [35, 36], and (b) detection of arterial wall with a threshold method. The decision on what technique to use is typically based on the quality of the medical data and availability of proper software, however, at the present time there is no preferred method [37]. All methods have the same weakness in automatically distinguishing between vessel bifurcation and vessel fusion generated as an artifact in the image, as well as in the ability to separate between adjacent bones and vessels. Another weakness of current automated arterial network reconstruction is in removing some features, such as presence of small vessels that are not supposed to be included in the simulation or, otherwise, in dealing with incomplete data when a part of the vessel is not seen [38]. To alleviate the aforementioned difficulties we developed a software package named *gOREK* [40] with a user-friendly Graphic User Interface, which allows the researcher to interact with medical data and to choose an appropriate numerical routine for reconstruction. The software is written in MATLAB, and this provides additional flexibility to even inexperienced users in implementing new features. The results shown in figure
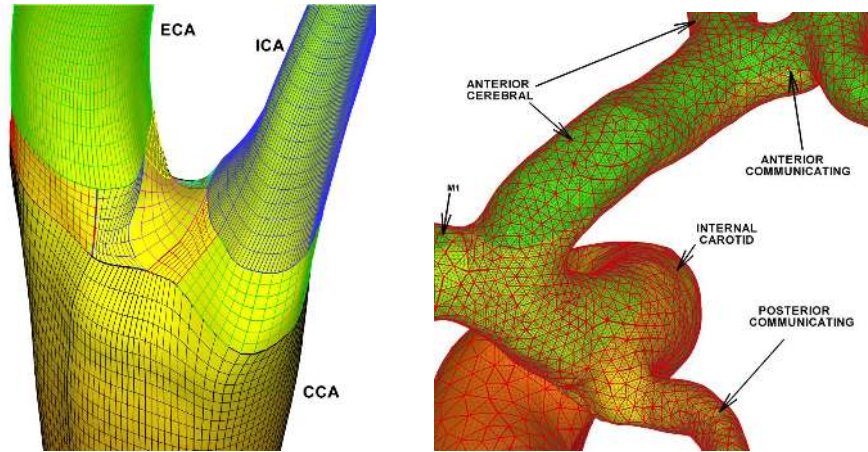
Figure 2: Left: Common, External and Internal Carotid Arteries (CCA, ECA and ICA) reconstructed from MRA data. The arterial wall is represented by parametric surfaces. Right: Cranial arterial network: The geometrical model was reconstructed from MRA and DSA CT images. Smoothing of the surface boundary was done with a technique described in [39].

1 as well as all results presented in this paper were based on gOREK reconstruction. The end-product of gOREK is a data set which determines the vessel shape and it can be used by *Gridgen* (Pointwise) [41] – a commercial mesh generator for additional editing and construction of finite element meshes.

In figure 1(top right) we present an example of a cranial arterial model reconstructed from MRA and DSA CT images. The model has 65 arteries, 4 inlets and 31 outlets. Due to high complexity of the arterial network, which also includes vessels of different sizes, several numerical approaches to reconstruct the vessel wall geometries were integrated. The inner part of the arterial network (Circle of Willis, CoW) was reconstructed by extracting iso-surfaces from MRA data with predefined threshold. The left and right anterior cerebral arteries are located very close to each other and their iso-surfaces were merged, hence these arteries had to be digitally separated. The small vessels, such as posterior temporal, were reconstructed using another technique: initially, the arterial medial axis is computed and the vessel diameter along the medial axis is approximated. Then, ring-like contours are seeded along the medial axis to form a pipe-like structure. Once all parts of the arterial tree were extracted the data were uploaded into *Gridgen*, where additional editing was performed to integrate all parts into one smooth surface, eliminate remaining small features, and form the inlet and outlet regions of the arteries. As a final step, a finite element mesh was generated. In figure 2(left) we plot the surface of a carotid artery bifurcation, reconstructed from a set of MRA images. The arterial wall is represented by several patches of a parametric surface. The surfaces corresponding to the arterial branches were generated by gOREK while the smaller patches were created in *Gridgen*.

Arterial geometry in NEKTAR: Our group has developed and used the CFD

code NEKTAR, which implements the high-order spectral/*hp* element method for spatial discretization of the computational domain [42]; the method provides very high spatial resolution and is suitable for complex geometries. Spectral/*hp* element method provides a dual path to convergence (i.e. decay of numerical error): (a) *h-convergence*, with the accuracy of the solution depending on the size of elements; and (b) *p-convergence* with the accuracy depending on the order of polynomial approximation and on the smoothness of the approximated solution. In the case of a smooth solution, exponential rate of convergence is obtained. The unstructured *surface mesh* generated using any meshing technique is an ensemble of many *flat* triangular or quadrilateral elements. The sharp angles, created by the merging of the surface elements may affect adversely the smoothness of the approximated solution leading to poor *p*-convergence. To recover exponential convergence, the flat surfaces of boundary elements can be mapped on curved (smooth) arterial wall surfaces. This points to the importance of a *consistent mesh generation* procedure. The surface mesh must be generated on a *smooth surface* provided by a geometric database, extracted during image processing. Then, the same database must be used to map a flat elemental surfaces on a curved boundary [43, 44]. In the case of the carotid artery, illustrated in figure 2(left), the parametric surfaces were used for mesh generation and subsequently for projection of faces of the boundary elements on the smooth surface. However, it was observed that if the original geometric database suffers from some degree of roughness then it cannot be used for projection of flat surfaces. In such cases, alternative methods for surface smoothing are available [39]. In our numerical algorithms we use a combination of techniques. The plot in figure 2(right) demonstrates a part of the geometric model of the cranial arterial network. The spectral element mesh was created using the smoothing technique described in [39].

Boundary conditions

Simulations of flow in domains with multiple inlets and outlets typically require two types of boundary conditions: (a) velocity boundary conditions at *all* inlets of the arterial network, and (b) velocity and pressure boundary conditions at *all* outlets. In patient-specific simulations the boundary conditions can be provided by measuring the velocity field at the inlets and outlets of the domain of interest. The pressure condition is inferred or assumptions are employed to extract it but it is preferable to have direct measurements of pressure if possible. The accuracy and completeness of imposed boundary conditions is crucial in CFD biomedical simulations and affects the results more significantly than numerical discretization errors do.

Typically, the Womersley velocity profile[45] for pulsatile flows is used as inflow boundary condition but it is only an approximation. The Womersley velocity profile is an analytical solution for unsteady pipe flow driven by a periodically time-varying pressure gradient. This velocity profile can be reconstructed from a given (measured) flowrate. It is axisymmetric and uni-directional, unlike the realistic

velocity distributions in arteries which are non-axisymmetric and involve all three velocity components. The effects of asymmetry in the inlet boundary condition was investigated in [46, 47] and significant differences in the downstream velocity fields were obtained with different inlet profiles. The effect of inlet boundary condition for cerebral aneurysms – specifically the proximity of an inlet to the location of the aneurysm – was also investigated in [48]; it was found that for the fusiform aneurysm there was a 100% wall shear stress (WSS) variation by changing the inflow profile, for fixed flowrate.

The importance of outflow boundary conditions has been long recognized by the community and the large literature reflects that [49, 50, 28, 51, 52]. As an example, let us assume that we want to simulate flow in the common carotid artery, which bifurcates to the internal and external carotid arteries (ICA and ECA). We also assume that the geometry of the artery was accurately reconstructed from CT or MRA data, and a physiologically correct inlet velocity profile, based on clinical measurements, is also provided. In order to start the numerical simulation, information about the flow states at all the outlets is required, but this information is typically missing. The outflow boundary conditions will determine to a large extent what percentage of a flow will enter the internal or external carotid artery. It is possible to set-up outlet boundary conditions such that 50% of blood will flow in each branch, but it is also possible to set-up the outlet boundary condition such that one of the arteries will be totally blocked. In the absence of physiologically correct (or patient-specific) outflow boundary condition, the results of such numerical simulations may be unrealistic. Progress can be made, however, by inferring the missing data from 0D or 1D models as we explain later. However, these models also require some knowledge of the patient-specific arterial topology, e.g. the dimensions of several generations of vessels starting from ICA and ECA. Here we have considered an example of a flow in rather simple arterial network - one inlet and two outlets. It is clear that in a case of more a complex network, such as the one presented in figure 1, the problem of the boundary conditions is much more complicated.

One of the most common outflow boundary conditions corresponds to fixing the pressure and assuming zero flux conditions for the velocity; such conditions are correct in the case of fully-developed laminar flow. In particular, the four main approaches for specifying the pressure at arterial outlets are:

- *Constant pressure boundary condition*: This type of boundary condition is reasonable for simulations of *steady* flows in a domain with a single outlet and also for *steady* flow simulations in domains with multiple outlets, provided that the pressure at each outlet is known from measurements.

- *Resistance boundary condition:* The Resistance boundary condition (R-BC) is based on the assumption of linear dependence between the pressure and flowrate at each outlet. R-BC has been applied by many researchers for flow simulation in 1D domains with multiple outlets, see [28, 50, 51].

- *Windkessel model boundary conditions:* There are several variations of the

9

Windkessel model for boundary conditions. The most common is the *three element* Windkessel model, which is often denoted as RCR model [51, 53, 54]. There are also variations of the Windkessel model where the inductance L is integrated in addition to resistance and capacitance [55].

- *Impedance boundary conditions:* This type of boundary condition was investigated in [49, 56], and it involves an analytical approach for modeling the outflow boundary conditions. More recently, new results with the impedance boundary condition were presented in [28, 52].

The Resistance, Windkessel and the Impedance boundary conditions are simply models developed to approximate the peripheral arterial network, hence avoiding the expensive simulations of the MeN/MiN systems. Implementation of these models usually requires iterative tuning of many parameters, which makes the CFD simulations computationally expensive.

To this end, next we present a new *scalable* and *efficient* type of pressure boundary condition applicable to vascular flow simulations in domains with multiple outlets [57]. Our method is *not* a new model that attempts to mimic the peripheral resistance but rather a numerical procedure that allows us to impose accurately and in a straight-forward manner measured *in-vivo* flowrates at terminal outlets. Measuring the flowrate, unlike measuring pressure, is a simple and harmless procedure that can be performed (for most of the arteries) within minutes using non-invasive techniques. Here we review two such techniques:

Transcranial Doppler (TCD) Ultrasound is the most commonly used method for assessing intracranial blood flow. The method was introduced by Aaslid *et al.* [58, 59] in the late 1980s. TCD is a non-invasive and harmless procedure, generally used to evaluate intracranial stenosis, cerebral arteriovenous malformations, cerebral vasospasm and cerebral hemodynamics [60]. In order to impose inflow/outflow boundary conditions in simulations of flow in an arterial network with multiple branches, the data collected with TCD at different arterial segments must be synchronized. Such synchronization can be performed by recording simultaneously Electrocardiogram (ECG) signal. A complete synchrony between signals of TCD data collected from multiple vessels is achieved by aligning the velocity peaks with the peaks in the corresponding ECG signals. The main drawback of ultrasonographic devices is their inability to penetrate bones. Hence, ultrasonography of the adult brain is very limited to areas which are not obscured by thick bone structures. Moreover, ultrasound only picks up the velocity component perpendicular to the ultrasound probe head, and the flow cannot be monitored in all directions simultaneously.

Phase-contrast (PC) MRI is a technique which overcomes the difficulties posed by TCD ultrasound [61]. PC MRI can be utilized for blood flow measurements in vessels which are inaccessible by TCD ultrasound, e.g., anterior and posterior cerebral and basilar arteries, superior sagittal sinus, etc. Moreover, the high-resolution PC MRI technique allows one to acquire *all three principal components* of blood flow

at multiple instances over the cardiac cycle. An example of PC MRI image of a coronal section at mid C2 level obtained from a healthy volunteer is shown in figure 3, along with the corresponding velocity field reconstruction. The reconstruction of the velocity fields from color-Doppler ultrasound (CDUS) or PC MRI is described in [38]. Volumetric flowrates are obtained by integration of the velocities throughout a lumen cross-sectional area defined by its boundary. The derived waveforms can be readily utilized in CFD simulations as inflow/outflow boundary conditions.
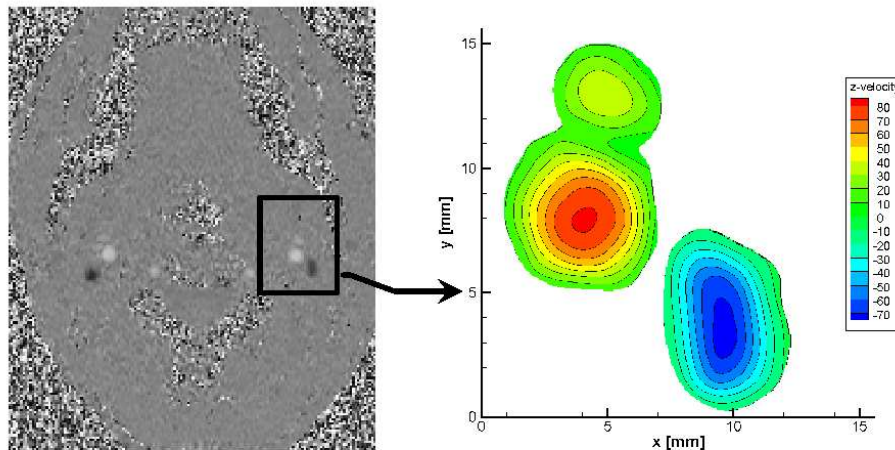

Figure 3: PC MRI-based velocity field reconstruction: Left: Phase-contrast MR image of blood flow at mid C2 level. Bright and dark circular spots enclosed into square section indicate the location of an artery and a vein. Right: map of the normal to the plane velocity component (in cm/s) in the artery (positive values) and in the vein (negative values).

In the following we describe briefly the numerical approach we developed to impose the pressure at the outlet boundaries. This approach is valid for steady and unsteady flow simulations and it is based on defining relative resistances at the domain outlets as functions of inverse ratio of their flowrates. For example, in a domain with two outlets the resistance values are computed from

$$R_2(t) = R_1 \frac{Q_1(t)}{Q_2(t)},$$

where Q_j are measured at outlets flowrates and $R_1 > 0$ is an arbitrary resistance at the first outlet. Then, the pressure at outlet j is computed from

$$P_j(t) = -R_j(t)C_j \frac{dP_j}{dt} + R_j(t)Q_j(t),$$

where C_j is a capacitance added to enhance the stability of the method. In our simulations the capacitance value is $C_j \approx 0.2/R_j$ and $R_1 \approx 100$. In general, the values of R and C represent the peripheral resistance and capacitance of the

11

arterial network. In our model the values are based on numerical considerations only: the resistance is computed from the measured Q_i/Q_j ratio while the value of the capacitance enhances the numerical stability. In figure 4 we present results of numerical simulation of unsteady flow in a network consisting of 20 cranial arteries. The results show very good agreement between the numerically computed and the imposed flowrates. The imposed (reference) flowrates where generated in a separate simulation with the Impedance boundary condition.
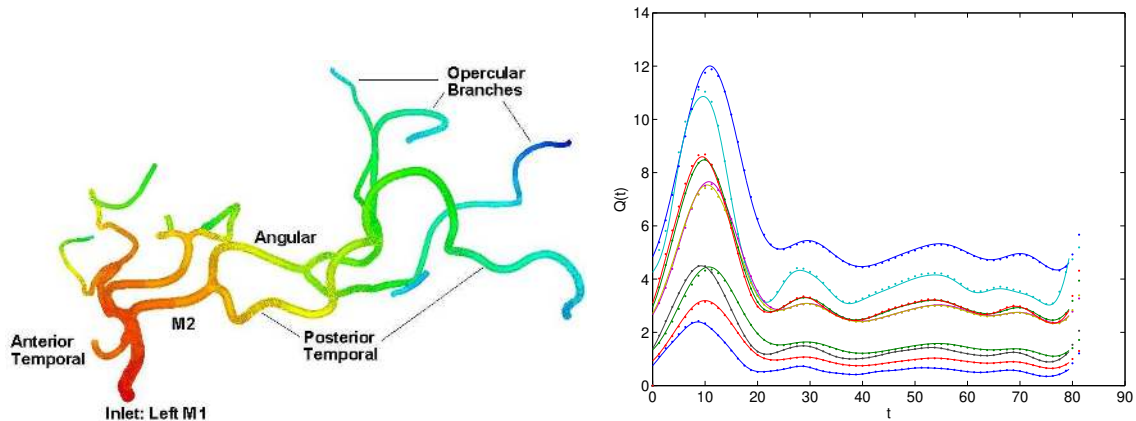

Figure 4: Unsteady flow simulation in a domain of 20 cranial arteries with time-dependent resistance boundary conditions. Left: computational domain; colors represent pressure distribution; red - high pressure, blue - low pressure. Right: flowrates at 10 outlets; solid line - reference flowrates, dot line - computed flowrates; Q(t) - non-dimensional flowrates at outlets, t - non-dimensional time.

NUMERICAL MODELS

The human arterial tree is composed of vessels with variable length and diameter. The largest artery in the human body is the aorta with a diameter of $3 - 5cm$ while the diameter of the smallest vessels, the capillaries, is typically $3 - 6\mu m$. The wide range in the size of the vessels has led to different numerical models for blood flow simulations [62]. In the past, the lack of sufficient computing power led to development of low-dimensional numerical models, e.g., lumped or 0D and 1D model. In the last two decades, CFD simulation of 2D and 3D arteries has been the more standard approach in analyzing blood flow. The multiscale nature of the arterial tree suggests *coupling* of low-dimensional models with more complex 3D simulations. In this section, we present such mixed numerical models for simulating the macro-vascular network (MaN) and a possible numerical extension that will make full 3D simulations of the arterial tree feasible in the near future.

0D, 1D and 3D modelling of a blood flow

The *zero-dimensional* (0D) model (also known as a lumped model) is based on the analogy between the current in an electric circuit (composed of a combination of resistors, capacitors and inductors) and the flowrate in blood vessels. An example of 0D model implementation can be found in [63], where the 0D model, representing a part of the circulatory system, was coupled to higher dimensional models. Often, lumped models are used in the "closure problem" for modeling the peripheral vascular network, in essence, providing a relationship between flowrate computed at the outlet of terminal vessel and pressure [28, 51, 52, 64].

The *one-dimensional* (1D) model has gained popularity due to its ability to predict with reasonable accuracy the pulse wave propagation. The 1D model is computationally inexpensive and can be applied successfully in simulations where blood flow does not exhibit strong 3D effects, e.g., in straight vessels with diameter less then 2mm. It can also be applied to simulate the pulse wave propagation in large vessels, however, only large scale features can be predicted, i.e., no information on the local flow dynamics is obtained [65]. An overview and examples of 1D modeling of blood flow can be found in [50, 64, 66]. The 1D models incorporate elastic properties of the arterial walls; a recent study accounts also for the *variability* of the elastic properties in the 1D model using stochastic modeling [67].

Computationally, the most expensive component is the *three-dimensional* (3D) modeling, which is essential in capturing secondary flows, turbulence, recirculation zones etc. Due to the geometric complexity of the arterial system, finite element or high-order spectral/hp element methods are preferred in solving the governing flow equations. A key numerical issue in 3D large-scale simulations is the use of fast parallel solvers scalable to thousands of processors [68, 69, 70]. As an example of 3D flow complexity, in figure 5(left) we present results from a numerical simulation of a flow in a stenosed carotid artery. In figure 5(right) we plot the monitored flowrate, $Q(t)$, at the tree branches and also the streamwise velocity component along the ICA branch. The high frequency oscillations (localized in time) indicate the presence of turbulent flow, in particular, the transition to turbulence and relaminarization during the systolic and diastolic phases, respectively.

0D-1D-3D coupling methods

Coupling of 0D, 1D and 3D simulations allows simulations of larger networks, which provides a better understanding of the interactions of the local 3D flow features with the effects of peripheral flow. The 3D sub-domain integrated in the 1D network can be used in capturing the complex flow patterns around arterial bifurcations [71]. The 0D models are incorporated to provide boundary conditions at the outlets or inlets of 1D domains. Coupling between these models is achieved by providing proper boundary conditions defined at the domain interfaces, [63, 72, 73]. Mathematically, this is not a trivial issue as it involves coupling of heterogeneous mathematical models,
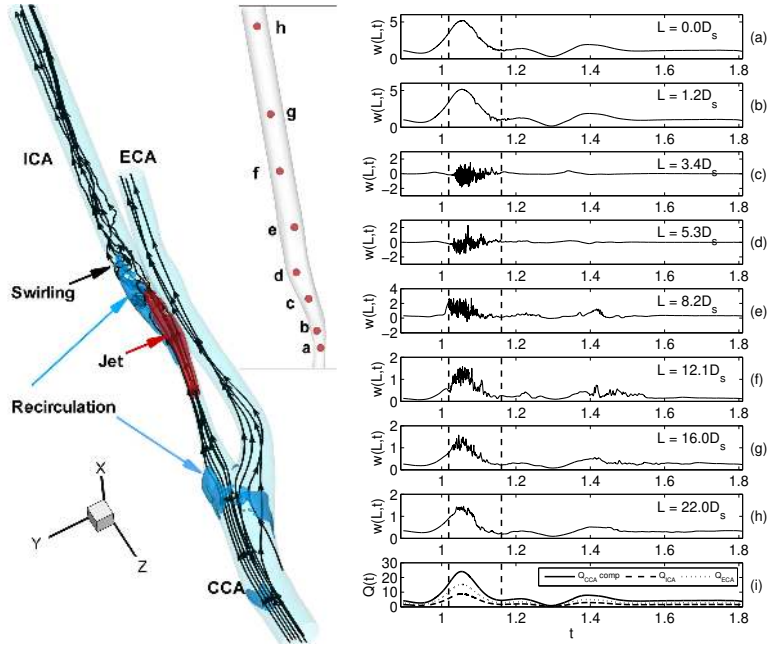
Figure 5: Flow patterns in a stenosed carotid artery. Left: Red iso-surfaces depict high speed flow region (jet), blue iso-surfaces show regions of backflow. Instantaneous streamlines demonstrate swirling flow. Right: flowrates and streamwise component of the velocity field monitored at distance L from the ICA narrowing (the selected history points are marked by the red dots). D_s - diameter of the ICA at the narrowest section. Dash lines - separate time frames of laminar and turbulent regimes.

e.g. parabolic equations (the 3D Navier-Stokes equations) coupled to hyperbolic 1D equations.

3D-3D coupling

The straight-forward 3D approach for the full-scale human arterial tree simulation, where a *single computational domain* is employed, is very inefficient and not scalable. The main difficulty is in the solution of a system of equations with billions of degrees of freedom. The reasons are both computational and algorithmic. From the computational standpoint, the high volume of communication between tens of thousands of processors affects adversly the efficiency of the parallel solver. From the algorithmic standpoint, the solution of linear systems involves dense matrices of rank above one billion with extremely large condition number, hence requiring thousands of iterations per time step for convergence.

To this end, we decompose the arterial network into a series of loosely coupled sub-domains of manageable size by providing appropriate interface conditions between sub-domains. Subsequently, the entire simulation can be performed on two levels: (i) in the inner level we solve a series of *tightly coupled* 3D problems in each

14

sub-domain, and (ii) in the outer level we solve *loosely coupled* problems by imposing proper boundary conditions at the sub-domains interfaces.

Multi-level partitioning of the entire computational domain requires multi-level parallelism in order to maintain high parallel efficiency using thousands of processors. Typically, we use 4-5 layers of processor sub-groups when computing on a single supercomputer center and an additional layer when computing on a network of distributed supercomputers, such as the TeraGrid [74, 75]. The interface boundary conditions required for coupling 3D sub-domains are computed explicitly and include the velocity boundary condition at the inlets of computational sub-domains along with pressure and flux at the sub-domain outlets. At the inlet, of the downstream vessel the velocity boundary conditions are provided by the upstream vessel, i.e.

$$\mathbf{V}^{n+1}|_{inlet} = \mathbf{V}^n|_{outlet},$$

where the superscripts denote time steps. The pressure at the sub-domain outlet is given by

$$P^{n+1}|_{outlet} = F(t)\bar{P},$$

where $\bar{P} = 0.5(P^n|_{inlet} + P^n|_{outlet})$, $F(t) = (1 - e^{-\alpha t^{n+1}})^\beta$ and α and β are positive constants. The filter function $F(t)$ suppresses large pressure oscillations that may appear at the beginning of the simulation due to poor choice of the initial velocity field (in our simulations we used $\alpha = 20$ and $\beta = 2$). The flux at the upstream sub-domain outlet is computed as an average of the normal velocity derivatives from both sides of the interface, i.e.,

$$\frac{d\mathbf{V}^{n+1}}{dn}\bigg|_{outlet} = \frac{1}{2}\left(-\frac{d\mathbf{V}^n}{dn}\bigg|_{inlet} + \frac{d\mathbf{V}^n}{dn}\bigg|_{outlet}\right).$$

We note that the error introduced by the explicit treatment of the interface boundary conditions is controlled by the size of time step.

Next, we present two large-scale numerical simulations using coupled 3D-3D-0D models. Our primary goal in these simulations is to test this new 3D-3D-0D coupling method. In both cases the three-dimensional computational domain was decomposed into four sub-domains coupled by the interface boundary conditions. The *RC*-type pressure boundary conditions at the terminal vessels were employed, which allowed us to control the flow distribution across multiple branches. The computational domain was discretized with tetrahedral spectral elements, and the solution was approximated with polynomial order $p = 5$ and $p = 6$. The computational details are summarized in table 1. Both simulations were performed on the CRAY XT3 of the Pittsburgh Supercomputing Center (PSC). We performed a steady flow simulation in the domain of the aorta shown in figure 6(left) and a time-dependent flow simulation in the cranial arterial network in figure 6(middle and right). The estimated computational time required for solution of the unsteady flow in a domain of 65 cranial arteries over *one cardiac cycle* on 3,265 processors of CRAY XT3 is *80 hours*, a rather reasonable time for supercomputing applications.
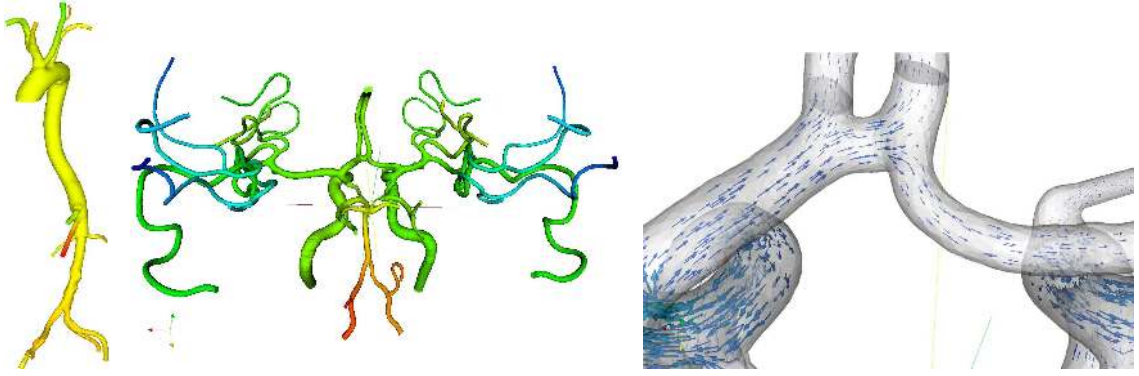
15

Figure 6: Large-scale flow simulations of the human arterial tree. Left: Aorta and adjacent arteries; 20 arteries, 1 inlet, 13 outlets; reconstruction from CT images; colors represent pressure distribution: red - high pressure, blue - low pressure. Middle: Cranial arterial network; 65 arteries, 4 inlets, 31 outlets; reconstruction from MRA and DSA CT images; colors represent pressure distribution. Right: Flow pattern in the Circle of Willis. Arrows depict the instantaneous flow direction. The simulation indicates that during part of a cardiac cycle blood supplied through the left ICA feeds booth hemispheres of the brain.

Table 1: Large-scale flow simulations in the human arterial tree: Computational details. Simulations were performed on the CRAY XT3 at PSC. Nel - number of spectral elements, p - polynomial order, DOF - number of degrees of freedom, Ncpu - number of processors, CPU-time - averaged computer time required for one time step.

Domain	Nel	p	DOF (per variable)	Ncpu	CPU-time
Aorta	325,795	6	187,657,920	1976	0.77 sec
Cranial arterial network	459,250	5	180,026,000	3265	0.61 sec

OUTLOOK

Multiscale modeling of the virtual physiological human (VPH) has attracted a lot of attention recently and several efforts are currently underway to address many aspects of this problem in USA, Europe and Japan; project descriptions have been published on-line in [76]. Simulating blood flow in the entire arterial tree is an indispensable component of VPH modeling and perhaps the most complex one from the computational standpoint. We discussed in the Introduction section how a hierarchical approach that couples MaN-MeN-MiN can possibly lead to an efficient simulation of the human arterial tree on the new emerging petaflop systems

16

with hundreds of thousands of processors. In order to estimate the computational resources required for a full-scale simulation we can extrapolate from the results obtained in the previous section for MaN. To make the discussion specific we consider here only the *cerebral vascular network* and we include modeling of both MeN and MiN; modeling of the entire tree will require roughly ten times more resources. In particular, we will assume that we will employ a 1D model to simulate MeN and Darcy's law (a phenomologically derived constitutive equation that describes the flow of a fluid through a porous medium) to simulate perfusion in MiN. To this end, we assume that: At the MaN level to model about 100 arteries (using the 3D spectral/hp element method [42]) requires 5 million spectral elements and hence 1 second per time step on 40,000 processors, or *27.7 (wall-clock) hours per cardiac cycle.* Based on this CPU requirement, we will select the number of processors for the other two levels of computation. Specifically, MeN can be modeled via the nonlinear 1D PDE system [64] and a discontinuous Galerkin discretization [77]. Each arteriole is represented by a 1D spectral element for a total of 10 million elements and 100 stochastic simulations. Employing 40,000 processors for the MeN simulations leads to 27.7 (wall-clock) hours per cardiac cycle, and hence it matches the CPU time for the MaN simulation. Finally, we should employ three sets of simulations (in three different brain regions) for solving the stochastic Darcy's law using "effective" values of diffusivity [78, 79] – and having fixed the time at 27.7 (wall clock) hours per cardiac cycle – we need $3 \times 10,000 = 30,000$ processors. In terms of *memory requirements* (accounting for the coupled stochastic simulations, co-processing for analysis and visualizations, and in-memory checkpointing) we estimate that for modest resolution we require more than 100 TBs while doubling the resolution will lead to more than 500 TBs.

In summary, we estimate that a single multiscale simulation of the human brain vascular network will require about 27.7 wall-clock hours per cardiac cycle on 110,000 processors; such systems are currently available but they may not have sufficient memory (see www.top500.org). Hopefully, on systems with 500,000 processors or more the required wall-clock per cardiac cycle will be of no more than 6 hours (and will satisfy the memory requirements) – a very reasonable simulation indeed! This will then open up the possibility of systematic studies in investigating clinical pathologies that will involve several cardiac cycles. However, there is much more modeling complexity to be added in the VPH, including blood rheology, biochemistry, blood-endothelium interactions, etc., which will make such full-scale simulations intractable even on the next generations of hexascale computers.

Acknowledgment

References

[1] Taylor CA, Draney MT, Ku JP et al. Predictive medicine: Computational techniques in therapeutic decision-making. *Computer Aided Surgery* 1999; **4**(5):231-247.

[2] Jackson MJ, Bicknell CD, Zervas V *et al.* Three-dimensional Reconstruction of Autologous Vein Bypass Graft Distal Anastomoses Imaged with Magnetic Resonance: Clinical and Research Applications. *Journal of Vascular Surgery* 2003; **38**(3):621-625, 2003.

[3] Wilson NM, Wang K, Dutton RW, Taylor CA. *Lecture Notes in Computer Science.* Springer Berlin/Heidelberg 2001; 2208:449-456.

[4] Ku JP, Draney MT, Arko FR, Lee WA *et al.* In Vivo Validation of Numerical Predictions of Blood Flow in Arterial Bypass Grafts. *Annals of Biomedical Engineering* 2002; **30**(6):743-752.

[5] Wan J, Steele BN, Spicer SA *et al.* A One-dimensional Finite Element Method for Simulation-based Medical Planning for Cardiovascular. Disease *Computer Methods in Biomechanical Engineering 2002*; **5**(3):195-206.

[6] Bradbury M, Begley D, Kreuter J. The Blood-Brain Barrier and Drug Delivery to the CNS. *Informa Healthcare; 1st edition* 2000.

[7] Goldman D, Popel AS. A Computational Study of the Effect of Capillary Network Anastomoses and Tortuosity on Oxygen Transport. *Journal of Theoretical Biology* 2000; **206**(2):181-194.

[8] Lorthois S, Stroud-Rossman J, Berger S and et al. Numerical Simulation of Magnetic Resonance Angiographies of an Anatomically Realistic Stenotic Carotid Bifurcation. *Anna. Biomed. Eng* 2005; **33**:270-283.

[9] Marshall I, Zhao S, Papathanasopoulou P. et al. MRI and CFD Studies of Pulsatile Flow in Healthy and Stenosed Carotid Bifurcation Models. *J. Biomech.* 2004; **37**:679-687.

[10] Moore JA, Steinman DA, Ethier CR. Computational Blood Flow Modelling: Errors Associated with Reconstructing Finite Element Models From Magnetic Resonance Images. *J. Biomech.* 1998; **31**:179-184.

[11] Papathanasopoulou P, Zhao S, Koehler U, et al. MRI Measurement of Time-resolved Wall Shear Stress Vectors in a Carotid Bifurcation Model, and Comparison with CFD Predictions. *J. Magn. Res. Imaging* 2003; **17**:153-162.

[12] Steinman DA, Thomas JB, Ladak HM, et al. Reconstruction of Carotid Bifurcation Hemodynamics and Wall Thickness Using Computational Fluid Dynamics and MRI. *Magn. Res. Med.* 2002; **47**:149-159.

[13] Steinman DA, Vorp DA, Ethier CR. Computational Modeling of Arterial Biomechanics: Insights into Pathogenesis and Treatment of Vascular Disease. *J. Vasc. Surg.* 2003; **37**:1118-1128.

[14] Stroud JS, Berger SA, Saloner D. Numerical Analysis of Flow Through a Severely Stenotic Carotid Artery Bifurcation. *J. Biomech. Eng.* 2002; **33**:9-20.

[15] Just A, Ehmke H, Wittmann U, Kirchheim HR. Role of Angiotensin II in Dynamic Renal Blood Flow Autoregulation of the Conscious Dog. *Journal of Physiology* 2002; **538**(1):167-177.

[16] Tofteng F, Hauerberg J, Hansen BA, Pedersen CB, Jorgensen L, Larsen FS. Persistent Arterial Hyperammonemia Increases the Concentration of Glutamine and Alanine in the Brain and Correlates with Intracranial Pressure in Patients with fulminant Hepatic Failure. *Journal of Cerebral Blood Flow & Metabolism* 2006; **26**:2127.

[17] Just A, Arendshorst WJ. A Novel Mechanism of Renal Blood Flow Autoregulation and the Autoregulatory Role of A1 Adenosine Receptors in Mice. *Am J Physiol Renal Physiolgy* 2007; **293**(5):F1489 - F1500.

[18] Upton RN. Cerebral Uptake of Drugs in Humans. *Clinical and Experimental Pharmacology and Physiology* 2007; **34**(8):695701.

[19] Duckles SP, Krause DN. Cerebrovascular Effects of Oestrogen: Multiplicity of Action. *Clinical and Experimental Pharmacology and Physiology* 2007; **34**(8):801808.

[20] Born GVR. Aggregation of Blood Platelets by Adenosine Diphosphate and its Reversal. *Nature* 1962; **194**:927

[21] Pivkin IV, Richardson PD, Karniadakis GE. Blood Flow Velocity Effects and Role of Activation Delay Time on Growth and Form of Platelet Thrombi. *Proceedings of National Academy of Sciences of the United States of America* 2006; **103**:17164-17169.

[22] Fogelson A, Yu H, Kuharsky A. Computational Modeling of Blood Clotting: Coagulation and Three-dimensional Platelet Aggregation. *In: Polymer and Cell Dynamics: Multicsale Modeling and Numerical Simulations* Birkhuser, Basel 2003, 2003; 145-154.

[23] Cassot F, Lauwers F, Fouard C, Prihaska S, Lauwers-Cances V. A Novel Three-Dimensional Computer-Assisted Method for a Quantitative Study of Microvascular Networks of the Human Cerebral Cortex. *Microcirculation* 2006; **13**:1-18.

[24] Zamir M. On Fractal Properties of Arterial Trees. *Journal of Theoretical Biology* 1999; **197**(4):517-526.

[25] Murray CD. The Physiological Principle of Minimum Work. I The Vascular System and the Cost of Blood Volume. *Proc. Natl. Acad. Sci. USA* 1926; **12**:207-214.

[26] Sherman TF. The meaning of Murray's law. *J. Gen. Physiol.* 1981; **78**:431-453.

[27] Fischer PF, Loth F, Lee SE, Lee SW, Smith D, Bassiouny H. Simulation of High Reynolds Number Vascular Flows. *CMAME* 2007; **196**:3049-3060.

[28] Vignon-Clementel IE, Figueroa CA, Jansen KE, Taylor CA. Outflow Boundary Conditions for Three-Dimensional Finite Element Modelling of Blood Flow and Pressure in Arteries. *Comp. Meth. Appl. Mech. Eng.* 2006; **195**:3776-3796.

[29] Castro MA, Putman CM, Cebral JR. Patient-Specific Computational Fluid Dynamics Modeling of Anterior Communicating Artery Aneurysms: A Study of the Sensitivity of Intra-Aneurysmal Flow Patterns to Flow Conditions in the Carotid Arteries. *American Journal of Neuroradiology* 2006; **27**:2061-2068.

[30] Castro MA, Putman CM, Cebral JR. Patient-Specific Computational Modeling of Cerebral Aneurysms With Multiple Avenues of Flow From 3D Rotational Angiography Images. *Academic Radiology* 2006; **13**(7):811-821.

[31] http://www.teragrid.org

[32] Dong S, Karniadakis GE, Karonis NT. Cross-site Computations on the Tera-Grid. *Computing in Science and Engineering* 2005; **7**(5):14-23.

[33] Loeckx D, Coudyzer W, Maes F *et al.* Nonrigid Registration for Subtraction CT Angiography Applied to the Carotids and Cranial Arteries. *Academic Radiology* 2007; **14**(12):1562-1576.

[34] Lell M, Anders K, Klotz E, Ditt H, Bautz W, Tomandl BF. Clinical Evaluation of Bone-Subtraction CT Angiography (BSCTA) in Head and Neck Imaging. *European Radiology* 2006; **16**(4):889-897.

[35] Wang KC, Taylor CA, Hsiau Z, Parker D, Dutton RW. Level Set Methods and MR Image Segmentation for Geometric Modelling in Computational Hemodynamics. *Engineering in Medicine and Biology Society, 1998. Proceedings of the 20th Annual International Conference of the IEEE* 1998; **6**(29):3079 - 3082.

[36] Sethian JA. *Level Set Methods and Fast Marching Methods: Evolving Interfaces in Computational Geometry, Fluid Mechanics, Computer Vision, and Materials Science (2nd ed).* Cambridge University Press, Cambridge 1998.

[37] Moore JA, Steinman DA, Holdsworth DW, Ethier CR. Accuracy of Computational Hemodynamics in Complex Arterial Geometries Reconstructed from Magnetic Resonance Imaging. *Annals of Biomedical Engineering* 2004; **27**(1):32-41.

[38] Yakhot A, Anor T, Karniadakis GE. A Reconstruction Method for Gappy and Noisy Arterial Flow Data. *IEEE Trans. Med. Imaging* 2007; **26**(12):1681-1697.

[39] Volino P, Magnenat-Thalmann N. The SPHERIGON: A Simple Polygon Patch for Smoothing Quickly Your Polygonal Meshes. *Proceedings of the Computer Animation* 1998, 72-78.

[40] Grinberg L. Multiscale Modelling and Parallel Algorithms for the Cerebrovasculature. *PhD thesis*, Brown University, in progress.

[41] http://www.pointwise.com.

[42] Karniadakis GE, Sherwin SJ. *Spectral/hp Element Methods for CFD; Second edition.* Oxford University Press, Oxford. 2005.

[43] Peiró J, Giordana S, Griffith C, Sherwin SJ. High-order Algorithms for Vascular Flow Modelling. *International Journal for Numerical Methods in Fluids* 2002; **40**(1-2):137-151.

[44] Sherwin SJ, Peiró J. Mesh Generation in Curvilinear Domains Using High-order Elements. *International Journal for Numerical Methods in Engineering* 2002; **53**:207-223.

[45] Zamir M. The Physics of Pulsatile Flow. Springer, 2000.

[46] Peterson S, Plesniak M. Experimental Study of the Effect of a Skewed Inlet Flow Profile on Stenotic Flow Development, *59th Annual Meeting of the APS Division of Fluid Dynamics* 2006.

[47] Yang XL, Liu Y, So RMC, Yang JM. The Effect of Inlet Velocity Profile on the Bifurcation COPD Airway Flow. *Computers in Biology and Medicine* 2006; **36**(2):181-194.

[48] Baek H, Jayaraman MV, Karniadakis GE. Distribution of WSS on the Internal Carotid Artery With an Aneurysm: A CFD sensitivity study. *IMECE2007* 2007.

[49] Olufsen MS. Structured Tree Outflow Condition for Blood Flow in Larger Systemic Arteries. *Am. J. Physiol.* 1999; **276**:H257-H268.

[50] Sherwin SJ, Franke V, Peiró J, Parker K. One-dimensional Modelling of a Vascular Network in Space-time Variables. *Journal of Engineering Mathematics* 2004; **47**(3-4): 217-250.

[51] Formaggia L, Lamponi D, Tuveri M, Veneziani A. Numerical Modelling of 1D Arterial Networks Coupled with a Lumped Parameters Description of the Heart. *Computer Methods in Biomechanics and Biomedical Engineering* 2006; **9**(5):273-288.

[52] Spilker RL, Feinstein JA, Parker DW, Reddy VM, Taylor CA. Morphometry-Based Impedance Boundary Conditions for Patient-Specific Modelling of Blood Flow in Pulmonary Arteries. *Annals of Biomedical Engineering* 2007; **35**(4):546-559.

[53] Nichols WW, O'Rourke MF, Hartley C. *McDonald's Blood Flow in Arteries; Theoretical, Experimental and Clinical Principles. Fourth edition.* A Hodder Arnold Publication, 1998.

[54] Gibbons CA, Shadwick RE. Circulatory mechanics in the Toad Bufo Marinus: II. Haemodynamics of the arterial Windkessel. *Journal of Experimental Biology* 1991; **158**:291-306.

[55] Alastruey J, Parker KH, Peiró J, Sherwin SJ. Lumped Parameter Outflow Models for 1-D Blood Flow Simulations: Effect on Pulse Waves and Parameter Estimation. *Communications in Computational Physics* 2008; **4**:317-336.

[56] Olufsen MS, Peskin CS, Kim WY, Pedersen EM, Nadim A, Larsen J. Numerical Simulation and Experimental Validation of Blood Flow in arteries with structured-tree outflow conditions. *Annals of Biomedical Engineering* 2000; **28**:1281-1299.

[57] Grinberg L, Karniadakis GE. Outflow Boundary Conditions for Arterial Networks with Multiple Outlets. *Annals of Biomedical Engineering*, under review.

[58] Aaslid R, Markwalder TM, Nornes H. Noninvasive Transcranial Doppler Ultrasound Recording of Flow Velocity in Basal Cerebral Arteries. *J. Neurosurg.* 1982; **57**:769-74.

[59] Aaslid R, Huber P, Nornes H. A Transcranial Doppler Method in the Evaluation of Cerebrovascular Spasm. *Neuroradiology* 1986; **28**:11-6.

[60] Evans DH, McDicken WN, Skidmore R, Woodcock JP. Doppler Ultrasound: Physics. Instrumentation and Clinical Applications. Wiley, Chichester, 1989.

[61] Pelc NJ, Herfkens RJ, Shimakawa A, Enzmann D. Phase Contrast Cine Magnetic Resonance Imaging. *Magnetic Resonance Quarterly 4* 1991; 229-254.

[62] Taylor CA, Draney MT. Experimental and Computational Methods in Cardiovascular Fluid Mechanics. *Annu. Rev. Fluid Mech.* 2004; **36**:197-231.

[63] Formaggia L, Nobile F, Quarteroni A, Veneziani A. Multiscale Modelling of the Circulatory System: a Preliminary Analysis. *Computing and Visualization in Science* 2004; **2**(2-3):75-83.

[64] Alastruey J, Parker K, Byrd S, Peiró J, Sherwin SJ. Modelling the circle of Willis to Assess the Effects of Anatomical Variations and Occlusions on Cerebral Flows. *Journal of Biomechanics* 2007; **40**(8):1794-1805.

[65] Matthys KS, Alastruey J, Peiró J, et al. Pulse wave propagation in a model human arterial network: assessment of 1D numerical simulations against in-vitro measurements, *Journal of Biomechanics* 2007; **40**:3476-3486.

[66] Wang JJ, Parker KH. Wave Propagation in a Model of the Arterial Circulation. *Journal of Biomechanics* 2004; **37**(4):457-470.

[67] Xiu DB, Sherwin SJ. Parametric Uncertainty Analysis of Pulse Wave Propagation in a Model of a Human Arterial Network. *Journal of Computational Physics* 2007; **226**:1385-1407, 2007.

[68] Tufo HM, Fischer PF. Terascale Spectral Element Algorithms and Implementations. Gordon Bell Prize paper, Proceedings of the ACM/IEEE SC99 Conference on High Performance Networking and Computing. IEEE Computer Soc. 1999.

[69] Bergen B, Hulsemann F, Rude U. Is 1.7×10^{10} Unknowns the Largest Finite Element System that Can Be Solved Today? *Supercomputing. Proceedings of the ACM/IEEE SC 2005 Conference* 2005.

[70] Grinberg L, Pekurovsky D, Sherwin SJ, Karniadakis GE. Parallel Performance of a Low Energy Basis Preconditioner for Spectral/hp Elements. *Parallel Computing*, under review.

[71] Dong S, Insley J, Karonis NT, et al. Simulating and Visualizing the Human Arterial System on the TeraGrid. *Future Generation Computer Systems, The International Journal of Grid Computing: Theory, Methods and Applications* 2006; **22**1011-1017.

[72] Formaggia L, Gerbeaum JF, Nobile F, Quarteroni A. On the Coupling of 3D and 1D Navier-Stokes Equations for Flow Problems in Compliant Vessels. *Comp. Meth. Appl. Mech. Eng.* 2001; **191**:561-582.

[73] Urquiza SA, Blanco PJ, Vénere MJ, Feijóo RA. Multidimensional Modelling for the Carotid Artery Blood Flow. *Comp. Meth. Appl. Mech. Eng.* 2006; **195**(33-36):4002-4017.

[74] Grinberg L, Toonen B, Karonis N, Karniadakis GE. A New Domain Decomposition Technique for TeraGrid Simulations. *TG07*, 2007.

[75] Grinberg L, Karniadakis GE. Spectral/hp Element Simulation of the Human Arterial Tree on the TeraGrid. *USNCCM9* 2007.

[76] See web sites: www.physiome.org; www.europhysiome.org.

[77] Cockburn B, Karniadakis GE, Shu CW. Discontinuous Galerkin Methods: Theory Computation and Applications. Springer-Verlag, 2000.

[78] Whiteaker S. The Method of Volume Averaging. Kluwer Academic Publisher, 1999.

[79] Liang Z, Ioannidis MA, Chatzis I. Permeability and Electrical Conductivity of Porous Media From 3D Stochastic Replicas of the Microstructure. *Chemical Engineering Science* 2000; **55**(22):5247-5262.